Predicting Motion of Vulnerable Road Users using High-Definition Maps and Efficient ConvNets

Fang-Chieh Chou, Tsung-Han Lin, Henggang Cui, Vladan Radosavljevic,
Thi Nguyen, Tzu-Kuo Huang, Matthew Niedoba, Jeff Schneider, Nemanja Djuric
Uber Advanced Technologies Group
{fchou, hanklin, hcui2, vradosavljevic, thi,
tkhuang, mniedoba, jschneider, ndjuric}@uber.com

Abstract

Following detection and tracking of traffic actors, prediction of their future motion is the next critical component of a self-driving vehicle (SDV), allowing the SDV to move safely and efficiently in its environment. This task is particularly important when it comes to vulnerable road users (VRUs), such as pedestrians and bicycles. During SDV operations these actors need to be handled with special care due to an increased risk of injury, as well as the fact that their behavior is less predictable than that of motorized actors. We address this problem, and present a deep learning-based method for predicting future movement of VRUs. We build on our prior work, rasterizing high-definition maps and actor surrounding into top-view image used as input to convolutional networks. Moreover, we propose a fast architecture suitable for real-time inference, and present an ablation study of rasterization choices. Following successful tests the system was deployed to a fleet of SDVs.

1 Introduction

Recent advances in high-performance hardware and software led to unprecedented breakthroughs in AI applications, with a number of highly publicized success stories. Computers have reached and even surpassed human performance in centuries old games such as go and chess [28, 29], are starting to understand health conditions and suggest medical treatment [35], and can even reason about complex relationships conveyed through images [38]. This progress also prompted renewed enthusiasm and work on a technology with a potential to completely transform the way we live and work, namely self-driving cars (SDVs). While interest in SDVs goes as far back as the 1980s [23], only in the last decade government agencies and large industry players turned their focus towards the field, leading to a new era of research that caused leaps in real-world performance of SDVs [36].

Predicting actor movement is a critical part of the autonomous technology. Once a self-driving vehicle successfully detects and tracks a traffic actor in its vicinity, it needs to understand how they will move in the next couple of seconds for both actors and SDV to be safe during operation [5]. This particularly holds true for vulnerable road users (VRUs), defined as traffic actors with increased risk of injury, unprotected by an outside shield [20]. Road planners and policy makers have recognized this problem many decades ago, and attempted to mitigate it through several means. This included legal frameworks, designing new road types (e.g., segregating VRUs from motorized actors), educating both drivers and VRUs with particular focus on children and elderly that are at an even greater risk than others [4, 20], to name a few. These efforts have given limited results, and in the US proportion of VRUs within overall traffic deaths actually increased between 2008 and 2017 from 14% to 19%, proportion of deaths of all outside-of-vehicle actors increased from 20% to 33% between 1996 and 2017, while number of VRU fatalities in urban areas increased by staggering 46% since 2008 [18]. To reverse the negative trend observed on our streets we arguably need a new approach to this old problem, and development of VRU-focused self-driving technology has a potential to do exactly that.

Preprint. Work in progress.

In the current study we address a critical aspect of SDV technology, and focus on predicting motion for VRUs, namely pedestrians and bicycles. Our main contributions are summarized below:

- We present a system for motion prediction of VRU traffic actors, relying on recently proposed context rasterization techniques [5];
- We propose a fast convolutional neural network (CNN) architecture suitable for running in real-time onboard the SDV;
- We present an ablation study of various rasterization settings;
- Following extensive testing, the system was deployed to a fleet of self-driving vehicles.

2 Related work

Efficient and accurate detection, tracking and motion prediction of VRUs are one of the key factors for autonomous vehicles to be safely deployed in complex urban environments. With greatly improved detection and tracking of VRUs [21], research on motion prediction of VRUs has been gaining lot of traction recently. Most related work on VRU motion prediction focuses solely on pedestrians, although recent review of car-bicyclist accidents showed that bicyclists at crossings [3] and signalized intersections [32] are an important safety concern for SDVs. In this section we provide an overview of motion prediction of pedestrians and bicycles with respect to autonomous driving, while more comprehensive review that includes research on motion prediction of vehicles can be found in [5].

Motion prediction. A common approach for prediction of VRUs' motion in autonomous driving systems is to leverage motion model from tracking component and use it to predict future states of the VRUs. For example, most of the autonomous system's pedestrian tracking components use either the Brownian or the constant velocity motion models [31] that ignore the scene context that influences pedestrians' behavior. While these approaches work well for short-term motion predictions, they often fail in long-term prediction tasks that are critical for safe autonomous driving. Accuracy of long-term predictions can be improved by incorporating context features from the scene as VRUs' motion follows complex patterns constrained by static and dynamic obstacles along the path. Traditionally, hand-crafted features were used for motion prediction of VRUs' with respect to surrounding context. The social force model for pedestrian motion prediction incorporates interactive forces that guide pedestrians towards their goals and promote collision avoidance among pedestrians and between pedestrian and static obstacles [9, 40]. Similar approach was applied for bicyclist motion prediction [12]. [24] introduced a motion model for bicyclist motion prediction that incorporates knowledge of the road topology. The authors were able to improve the prediction accuracy by using specific motion models for limited set of canonical directions. [7] incorporated semantic features from the environment such as relative distance to curbside and status of pedestrian traffic lights in the Gaussian Process model and obtained more accurate predictions of pedestrian trajectories. A significant amount of research efforts has been devoted to modeling pedestrian motion using maximum entropy Inverse Reinforcement Learning (IRL) [42], introducing an IRL model based on a set of manually designed feature functions that represent interaction and collision avoidance behavior of pedestrians.

Deep learning motion prediction. While the standard motion prediction approaches are able to predict the pedestrian and bicyclist motions in many scenarios, the need for manual design of features makes them hard to scale in complex autonomous driving environments. Inspired by the success in the various areas of computer vision and robotics, many deep learning based approaches have been proposed recently for the motion prediction task in order to model relationships and influences which may not have been obvious how to represent manually. Most of deep learning approaches are based on LongShort Term Memory (LSTM) variant of recurrent neural networks (RNNs) [10] since a motion is a temporal sequence. [2] proposed an approach for pedestrian motion prediction using a LSTM network architecture and a "social pooling layer" that uses spatial information of nearby pedestrians to implicitly model interactions among them. [33] used a sequence-to-sequence LSTM encoder-decoder architecture to predict the pedestrian position and angle of direction. Incorporating the angular information in addition to the temporal information led to a significant improvement in the prediction accuracy. [37] proposed Social Attention method to predict future motion based on estimation of the relative importance of pedestrians through attention layer. In addition, [22] proposed an LSTM-based model for motion prediction that incorporates the map of static obstacles and encoding the surrounding pedestrians. Recently, [6] proposed LSTM-based Generative Adversarial Network (GAN) to generate and predict socially feasible motions. LSTM-based encoder-decoder

generator was used to predict the future motions while an LSTM-based discriminator that was used to predict whether each generated motion follows the social constraints. [25] presented a system named SoPhie for predicting trajectories based on GAN. By utilizing an RGB image from the scene and the trajectory information of the pedestrians, the method uses an LSTM-based GAN module to generate physically and socially acceptable trajectories. [17] incorporated scene information as well as human movement trajectories in the pedestrian motion prediction process. Unlike LSTM approaches, [19] proposed CNN-based approach where convolutional layers are utilized to handle temporal dependencies. The CNN-network is a sequence-to-sequence architecture where trajectory histories are used as inputs. However, this model does not use scene context information.

Efficient CNN architectures. Since the introduction of AlexNet [15], researchers made significant progress in improving the CNN architectures to make them more accurate and efficient. Improved architectures, such as VGG [30] or ResNet [8], tend to have a large number of layers running expensive computations, making them unsuitable for real-time inference. Recent proposals such as MobileNet [11] and ShuffleNet [41] replace regular convolutional operator with more efficient depthwise separable or group convolutions, making them small and fast for mobile applications. MobileNet V2 (MNv2) [26] further improves the original MobileNet by combining depthwise convolution with residual connections and bottleneck layers proposed in ResNet. One problem of this prior work is focus on reducing computational FLOPs instead of optimizing for inference latency on devices. More recently, MnasNet [34] applied network architecture search algorithms [43] to optimize MNv2 for both accuracy and inference latency on mobile devices, and is able to improve both while maintaining similar FLOPs. ShuffleNet v2 [16] proposed several guidelines for designing fast networks beyond counting FLOPs, and applied these guidelines to design architectures that are both fast and accurate on GPUs and mobile CPUs. In this paper we propose modifications to MNv2 that make it much faster on GPU without compromising accuracy.

3 Proposed approach

In this section we discuss our approach to trajectory prediction of VRU actors. Note that we followed the same setup used in our previous work [5] (originally applied to vehicle actors), where the same loss functions are used to train the CNN models. However, in this paper we demonstrate that the methodology can be successfully applied to VRU actors, and explore two aspects of the existing approach that are critical to model's accuracy and inference speed. First, we experimented with different variations of the CNN architectures, and proposed a novel architecture that reduces inference latency without affecting accuracy. Second, we performed ablation study of different rasterization configurations, and measured their impact on the prediction accuracy for VRU actors.

Let us assume that we have access to real-time data streams coming from sensors such as lidar, radar, or camera, installed aboard a self-driving vehicle. In addition, assume that these inputs are used by an existing detection and tracking system, outputting state estimates $\mathcal{S}$ for all surrounding actors (state comprises the bounding box, position, velocity, acceleration, heading, and heading change rate). Denote a set of discrete times at which tracker outputs state estimates as $\mathcal{T} = \{t_1, t_2, \ldots, t_T\}$, where time gap between consecutive time steps is constant (e.g., the gap is equal to $0.1s$ for tracker running at a frequency of $10Hz$). Then, we denote state output of a tracker for the i-th actor at time t_j as $\mathbf{s}_{ij}$, where $i = 1, \ldots, N_j$ with N_j being a number of unique actors tracked at t_j. Moreover, we assume access to detailed, high-definition map information $\mathcal{M}$ of the AV's operating area, including road and crosswalk locations, lane directions, and other relevant map information.

Using the state estimates and high-definition map, we rasterize an actor-specific bird's-eye view raster image encoding the actor's surrounding map and traffic actors for each actor of interest (see Figure 2 for examples). Then, given i-th actor's raster image and state estimate $\mathbf{s}_{ij}$ at time step t_j, we use a CNN model to predict its future state sequences up to H steps of horizon $[\mathbf{s}_{i(j+1)}, \ldots, \mathbf{s}_{i(j+H)}]$. Without the loss of generality, in this work we simplify the task to infer i-th actor's future x- and y-positions instead of full state estimates, while the remaining states can be derived by considering $\mathbf{s}_{ij}$ and the future position estimates. Both past and future positions at time t_j are represented in the actor-centric coordinate system derived from actor's state at time t_j, where forward direction is x-axis, left-hand direction is y-axis, and actor's bounding box centroid is the origin.

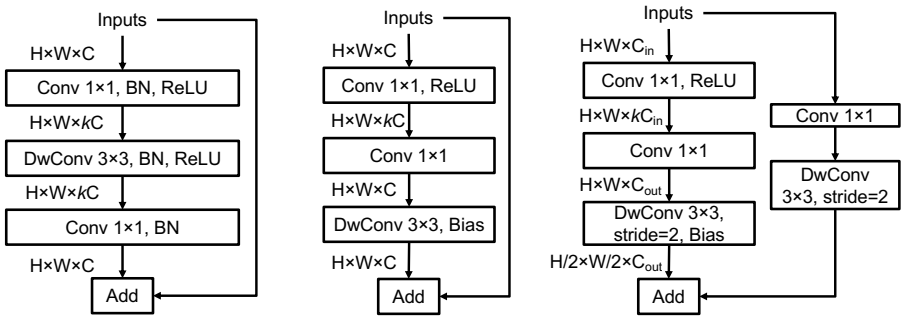

(a) Regular block of MNv2 (b) Regular block of FMNet (c) Stride=2 block of FMNet

Figure 1: Building blocks of MNv2 and FastMobileNet

Table 1: Base CNN architecture of FastMobileNet (upsample=6 for all FMNet blocks)

Layer	Output	Stride	Repeats
Raster image	$300 \times 300 \times 3$	–	–
Conv 3×3	$150 \times 150 \times 24$	2	1
DwConv 3×3	$75 \times 75 \times 24$	2	1
FMNet block 1	$75 \times 75 \times 12$	1	2
FMNet block 2	$38 \times 38 \times 16$	2	3
FMNet block 3	$19 \times 19 \times 32$	2	4
FMNet block 4	$19 \times 19 \times 48$	1	3
FMNet block 5	$10 \times 10 \times 80$	2	3
FMNet block 6	$10 \times 10 \times 160$	1	1
Conv 1×1	$10 \times 10 \times 640$	1	1
Global average pooling	$1 \times 1 \times 640$	1	1

3.1 Improved MNv2 architecture for fast inference

In this section we propose simple modifications to the MNv2 architecture that significantly speed up GPU inference. MNv2 is based on the inverted bottleneck block illustrated in Figure 1a. In each block, the input feature map is first up-sampled to k times more channels (k is set to 6 in the original MNv2) with 1×1 convolution, followed by 3×3 depthwise convolution (DwConv) applied to the up-sampled feature map. Then, the feature map is compressed back to the original channel size using 1×1 convolution, and summed with the initial input through residual connection. Non-linearity (e.g., ReLU) is applied only in the up-sampled phase, as non-linearity in the bottlenecked phase (before the up-sampling or after the compression) causes too much information loss and hurts model performance. Batch-norm (BN) is used in all 3 layers. While the majority of the FLOPs are in the 1×1 convolutions (i.e., 87%), the other operations are still non-negligible. As discussed in [16], FLOPs itself is not an accurate estimator of actual latency, and another important factor is the number of memory access operations (MAC). Operations such as DwConv, BatchNorm, ReLU, and BiasAdd, while having small FLOPs, typically incurs heavy MAC. Especially in MNv2, the operations in the up-sampled phase have k times more MAC than the same operations in the bottlenecked phase.

In the proposed novel architecture called FastMobileNet (FMNet), we move most of the operations originally in the up-sampled phase into the bottlenecked phase, reducing their FLOPs and MAC k times, see Figure 1b. The only remaining operation in the up-sampled phase is a ReLU. Similarly to MNv2, no ReLU is applied in the bottlenecked phase. As the layers are linear in the bottlenecked phase we only apply one BiasAdd at the end of the block, as applying multiple BiasAdd in consecutive linear layers does not increase model expressiveness. Note that we do not use batch-norm in FMNet as we found the model converges well during training without it, and excessive batch-norm operations cost additional computation time. The stride=2 block of FMNet is similar to the regular block (see Figure 1c), except the original input is downsampled to the correct output size for residual connection. The FMNet architecture before fully-connected and output layers (see [5] for more details) used in this work is shown in Table 1, where the layer sizes and block repeats of the model are based on MNv2-0.5 (i.e., MNv2 with halved channel sizes in all layers).

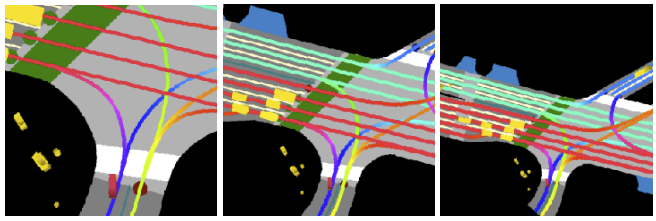

Figure 2: Raster images for bicycle actor (colored red) using resolution of 0.1m, 0.2m, and 0.3m

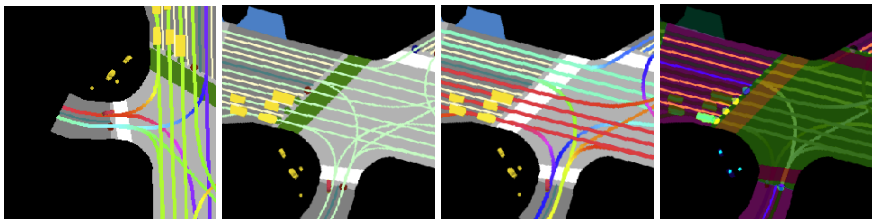

Figure 3: Different rasterization settings with 0.2m resolution for bicycle example: (a) no rotation, (b) no lane heading, (c) no traffic light, (d) learned colors

3.2 Rasterization

To describe rasterization, let us first introduce a concept of a *vector layer*, formed by a collection of polygons and lines that belong to a common type. For example, in the case of map elements we have vector layer of roads, of crosswalks, and so on. To rasterize vector layer into an RGB space, each vector layer is manually assigned a color from a set of distinct RGB colors that make a difference among layers more prominent. Once the colors are defined, vector layers are rasterized one by one on top of each other, in the order from layers that represent larger areas such as road polygons towards layers that represent finer structures such as lanes or actor bounding boxes. To represent context around the i-th actor tracked at time step t_j we create a rasterized image I_{ij} of size $n \times n$ such that the actor is positioned at pixel (w, h) within I_{ij}, where w represents width and h height measured from the bottom-left corner of the image. We color the actor of interest differently so that it is distinguishable from other actors.

In this study we tested several different choices of rasterization for the prediction of VRU actors. For all rasterization methods, we maintain a constant RGB raster dimension of 300×300 pixels (i.e., $n = 300$). The details of each rasterization choice are discussed below.

Raster frame rotation. In our previous work, we rotate the raster for each actor into the actor frame, such that the heading of each actor points up and the target actor is placed at $w = 150, h = 50$ (see Fig. 2). In this way heading of the actor is encoded directly into the input, and the raster encodes more context in front of the actor. We tested an alternative scheme where the raster frame is unrotated so that north direction points up, and the actor is placed in the center ($w = 150, h = 150$, see Fig. 3a).

Raster pixel resolution. The resolution governs the extent of surrounding context seen by the model. At $0.1m$ resolution, the model sees $25m$ in front and $5m$ behind the actor (assuming the rotated raster discussed above). Larger resolution allows for larger context around the actor, however the raster loses finer details which may be critical for accuracy. Thus, we experimented with resolutions of $0.1m$, $0.2m$ and $0.3m$, illustrated in Figure 2.

Lane direction. In our previous work, we encode the direction of each lane segment as a hue value in HSV color space, with saturation and value set to maximum, then convert HSV to RGB color space. Alternatively we can encode all lanes with a constant color, such that the raster does not contain lane direction information (see Figure 3b without using HSV approach, as opposed to Figure 2b).

Traffic lights. We use an existing traffic light classification algorithm to extract current traffic light states from sensor inputs. To encode this info in the input raster, we plot traffic light states as a colored circle at location where lane meets a traffic-light controlled intersection. Furthermore, we identify inactive crosswalks and paint them green (see Figure 3c without traffic light info, as opposed to Figure 2b). We tested if traffic light information impacts model accuracy.

Table 2: Comparison of base CNN architectures

Architecture	Pred. error [m]	Latency [ms]	FLOPs	Num. parameters
AlexNet	1.36	15.8	2.84G	70.3M
ResNet18	1.29	36.2	6.80G	11.7M
MNv2-0.5	**1.27**	21.3	**322M**	581k
MnasNet-0.5	1.28	18.3	335M	825k
FMNet	1.28	**12.1**	363M	**564k**

Learning raster colors. In our previous work, we manually picked colors for each raster layer type [5]. An alternative approach is to have the DNN learn the colors by itself. In this study, we provided all raster layers (e.g., road and vehicle polygons, tracked objects) as separate binary-valued channels to the network, and added a 1×1 convolution layer with 3 output channels and linear activation to generate the RGB raster image (see Figure 3d for example learned raster). The generated RGB image is then passed to the rest of the network as before.

Model pre-training. We also tested one modification not related to rasterization. As the majority of road actors are vehicles, our training dataset has a much larger number of such actors. We can thus initialize our VRU models with a pre-trained vehicle model trained using more examples. The model is then fine-tuned with VRU training examples until convergence.

4 Experiments

We collected 240 hours of data by manually driving SDV in Pittsburgh, PA and Phoenix, AZ in various traffic conditions (e.g., varying times of day, days of the week). The data contains significantly different number of examples for various actor types, namely 7.8 million vehicles, 2.4 million pedestrians, and 520 thousand bicycles. Traffic actors were tracked using Unscented Kalman filter (UKF) [39] with dynamic vehicle model [14], taking raw sensor data from the camera, lidar, and radar, and outputting state estimates for each object at $10Hz$. The filter is a default tracker on our fleet, trained on a large amount of labeled data, and tested on millions on miles (unfortunately, no other details can be given due to confidentiality concerns). We considered prediction horizon of $9s$ (i.e., $H = 90$) for VRU actors. For the default rasterization scheme (used in the following architecture experiments and as the baseline in the ablation study), we rotated raster to actor frame with resolution of $0.2m$, including both lane heading and traffic light raster layers.

We implemented models in TensorFlow [1] and trained on 16 Nvidia Titan X GPU cards. We used open-source distributed framework Horovod [27] for training, completing in around 24 hours. We used a per-GPU batch size of 64 and Adam optimizer [13], setting initial learning rate to 10^{-4} further decreased by a factor of 0.9 every $20{,}000$ iterations. Models were trained end-to-end from scratch.

4.1 Comparison of CNN architectures

In the first set of experiments we compared a number of CNN architectures, summarizing results in Table 2. We trained the models on vehicle actors and set the prediction horizon to $6s$. Average prediction error and latency are reported in the table. The inference latency is measured at a batch of 32 actors on a GTX 1080Ti GPU. As our prediction algorithm performs inference for each actor in the scene, having such a large batch size is not uncommon when SDV is driving on crowded roads.

We first compared the prediction accuracy and inference latency on several base CNN architectures. We found that our FMNet gives similar prediction accuracy as other modern architectures such as ResNet, MNv2 and MnasNet, while being much faster in inference. In terms of the number of FLOPs and parameters, FMNet is similar to MNv2-0.5 (which it is based on) and MnasNet-0.5, while AlexNet and ResNet18 have much more FLOPs and parameters. It is interesting to note that AlexNet is the second fastest CNN in our experiment while having large FLOPs (possibly because it has much fewer layers than other considered CNNs), although its accuracy is not on par with other networks. Following these results in the rasterization ablation studies we use FMNet as the model architecture.

Table 3: Comparison of prediction errors (in meters) for various experimental settings

	Bicycles			Pedestrians		
Experimental setup	**Average**	**@1s**	**@5s**	**Average**	**@1s**	**@5s**
UKF	2.89	0.80	6.60	0.67	0.22	1.22
Baseline	1.07	0.44	2.72	0.52	0.18	0.93
0.1m resolution	1.07	0.43	2.73	**0.51**	**0.17**	**0.90**
0.3m resolution	1.09	0.45	2.80	0.53	0.18	0.95
No rotation	1.29	0.49	3.30	0.58	0.20	1.02
No traffic lights	1.11	0.44	2.86	0.55	0.20	0.96
No lane headings	1.07	0.43	2.72	0.52	0.18	0.93
Learned colors	**1.05**	**0.42**	**2.70**	0.53	0.18	0.93
With car pretraining	**1.05**	**0.42**	**2.70**	0.59	0.20	1.05

4.2 Ablation studies on rasterization

We conducted a set of ablation studies regarding the rasterization setup, modifying various parameters of the rasterization configuration of the base setup. The empirical results are given in Table 3, where we see that the baseline CNN significantly outperforms UKF, especially at longer horizons.

First, we analyzed accuracy of the base 0.2m resolution, as compared to other resolution choices. Resolution of 0.1m has smaller coverage, and is expected to benefit slow-moving objects such as pedestrians. On the other hand, 0.3m resolution may benefit fast-moving objects requiring larger coverage. For pedestrians 0.1m-resolution indeed resulted in lower error, while setting 0.3m gave the worst performance. We observed that 0.1m showed no significant difference for bicycles, while 0.3m resulted in slightly higher error. This may be attributed to the fact that bicycles are not fast enough to benefit from larger context. Next, we evaluated the impact of not rotating raster such that actor heading points up, as discussed in Section 3.2, which resulted in a significant drop of accuracy for both actor types. This can be explained by the fact that, when raster is not rotated such that actor heading points up, there is a large number of input data variations that network needs to observe to learn how actors move. In other words, for such setup actors may move in any direction, which is not the case for rotated raster where actors always move upward initially resulting in a simplified prediction problem.

We further investigated the affect of encoding traffic light info. The traffic light is important for predicting longitudinal movement, as it can provide info about whether an actor may or may not pass through an intersection. We observed error increase without traffic light rasterization for both actor types, matching this intuition. Furthermore, we removed lane heading information provided in raster images, encoded by using different colors to indicate different directions. Without lane heading bicycle model degraded slightly in performance, while pedestrian model was unaffected. This again matches intuition, as bicycles may behave as vehicles and follow lane direction, while pedestrians do not normally use lanes. Finally, we tried learning raster colors instead of setting them manually. The results show that learned colors slightly improved accuracy of the bicycle model, whereas pedestrian model slightly degraded compared to the baseline. This indicates that our manual rasterization setup captured sufficient signal when it comes to pedestrians, while for bicycles it can be further improved.

Lastly, due to larger amount of vehicle data as compared to VRUs, instead of training from scratch we finetuned VRU models using preloaded weights from the vehicle model. The results show that bicycle performance improved over the baseline, indicating that bicycles may exhibit similar behavior to vehicles. On the other hand the pedestrian model regressed, which can be explained by the fact that pedestrian motion is very different from vehicle motion making vehicle pretraining ineffective.

5 Conclusion

In this paper we presented an efficient and effective solution to motion prediction of VRU traffic actors. This is a critical problem in autonomous driving, as such actors have higher risk of injury and are less predictable since they may change behavior faster than vehicles. We applied recently proposed rasterization technique to generate raster images of actors' surrounding encoding their context, which is then used to train deep CNNs to predict future trajectory. Moreover, we proposed a novel fast architecture suitable for real-time operations, and presented a detailed ablation study of

various rasterization choices. The results strongly indicate benefits of the proposed approaches over the state-of-the-art, which were deployed to a fleet of SDVs following extensive offline testing.

References

[1] M. Abadi, A. Agarwal, P. Barham, E. Brevdo, et al. TensorFlow: Large-scale machine learning on heterogeneous systems, 2015.

[2] A. Alahi, K. Goel, et al. *Social LSTM: Human Trajectory Prediction in Crowded Spaces*. IEEE, Jun 2016.

[3] I. Cara and E. d. Gelder. Classification for safety-critical car-cyclist scenarios using machine learning. In *2015 IEEE 18th International Conference on Intelligent Transportation Systems*, pages 1995–2000, Sept 2015.

[4] A. Constant and E. Lagarde. Protecting vulnerable road users from injury. *PLOS Medicine*, 7(3):1–4, 03 2010.

[5] N. Djuric, V. Radosavljevic, H. Cui, T. Nguyen, F.-C. Chou, T.-H. Lin, and J. Schneider. Short-term motion prediction of traffic actors for autonomous driving using deep convolutional networks. *arXiv preprint arXiv:1808.05819*, 2018.

[6] A. Gupta, J. Johnson, L. Fei-Fei, S. Savarese, and A. Alahi. Social gan: Socially acceptable trajectories with generative adversarial networks. *CoRR*, abs/1803.10892, 2018.

[7] G. Habibi, N. Jaipuria, and J. P. How. Context-aware pedestrian motion prediction in urban intersections. *CoRR*, abs/1806.09453, 2018.

[8] K. He, X. Zhang, S. Ren, and J. Sun. Deep residual learning for image recognition. In *Proceedings of the IEEE conference on computer vision and pattern recognition*, pages 770–778, 2016.

[9] D. Helbing and P. Molnár. Social force model for pedestrian dynamics. *Phys. Rev. E*, 51:4282–4286, May 1995.

[10] S. Hochreiter and J. Schmidhuber. Long short-term memory. *Neural Computation*, 9(8):1735–1780, 1997.

[11] A. G. Howard, M. Zhu, B. Chen, D. Kalenichenko, W. Wang, T. Weyand, M. Andreetto, and H. Adam. Mobilenets: Efficient convolutional neural networks for mobile vision applications. *CoRR*, abs/1704.04861, 2017.

[12] L. Huang, J. Wu, F. You, Z. Lv, and H. Song. Cyclist social force model at unsignalized intersections with heterogeneous traffic. *IEEE Transactions on Industrial Informatics*, 13(2):782–792, April 2017.

[13] D. P. Kingma and J. Ba. Adam: A method for stochastic optimization. *arXiv preprint arXiv:1412.6980*, 2014.

[14] J. Kong, M. Pfeiffer, G. Schildbach, and F. Borrelli. Kinematic and dynamic vehicle models for autonomous driving control design. In *Intelligent Vehicles Symposium (IV), 2015 IEEE*, pages 1094–1099. IEEE, 2015.

[15] A. Krizhevsky, I. Sutskever, and G. E. Hinton. ImageNet classification with deep convolutional neural networks. In *Advances in neural information processing systems*, pages 1097–1105, 2012.

[16] N. Ma, X. Zhang, H. Zheng, and J. Sun. Shufflenet V2: practical guidelines for efficient CNN architecture design. *CoRR*, abs/1807.11164, 2018.

[17] H. Manh and G. Alaghband. Scene-LSTM: A Model for Human Trajectory Prediction. *ArXiv e-prints*, Aug. 2018.

[18] NCSA. 2017 fatal motor vehicle crashes: Overview. Technical Report DOT HS 812 603, National Center for Statistics and Analysis, October 2018.

[19] N. Nikhil and B. Tran Morris. Convolutional Neural Network for Trajectory Prediction. *ArXiv e-prints*, Sept. 2018.

[20] OECD. Safety of vulnerable road users. Technical Report 68074, Organisation for Economic Co-operation and Development, Augist 1998.

[21] E. Ohn-Bar and M. M. Trivedi. Looking at humans in the age of self-driving and highly automated vehicles. *IEEE Transactions on Intelligent Vehicles*, 1(1):90–104, March 2016.

[22] M. Pfeiffer, G. Paolo, H. Sommer, J. Nieto, R. Siegwart, and C. Cadena. A data-driven model for interaction-aware pedestrian motion prediction in object cluttered environments. In *2018 IEEE International Conference on Robotics and Automation (ICRA)*, pages 1–8, May 2018.

[23] D. A. Pomerleau. Alvinn: An autonomous land vehicle in a neural network. In *Advances in neural information processing systems*, pages 305–313, 1989.

[24] E. A. I. Pool, J. F. P. Kooij, and D. M. Gavrila. Using road topology to improve cyclist path prediction. In *2017 IEEE Intelligent Vehicles Symposium (IV)*, pages 289–296, June 2017.

[25] A. Sadeghian, V. Kosaraju, A. Sadeghian, N. Hirose, S. H. Rezatofighi, and S. Savarese. SoPhie: An Attentive GAN for Predicting Paths Compliant to Social and Physical Constraints. *ArXiv e-prints*, June 2018.

[26] M. Sandler, A. Howard, M. Zhu, A. Zhmoginov, and L.-C. Chen. Mobilenetv2: Inverted residuals and linear bottlenecks. In *The IEEE Conference on Computer Vision and Pattern Recognition (CVPR)*, June 2018.

[27] A. Sergeev and M. D. Balso. Horovod: fast and easy distributed deep learning in tensorflow. *arXiv preprint arXiv:1802.05799*, 2018.

[28] D. Silver, A. Huang, et al. Mastering the game of go with deep neural networks and tree search. *Nature*, 529(7587):484–489, 2016.

[29] D. Silver, T. Hubert, et al. Mastering chess and shogi by self-play with a general reinforcement learning algorithm. *arXiv preprint arXiv:1712.01815*, 2017.

[30] K. Simonyan and A. Zisserman. Very deep convolutional networks for large-scale image recognition. *arXiv preprint arXiv:1409.1556*, 2014.

[31] L. Spinello, R. Triebel, and R. Siegwart. Multimodal people detection and tracking in crowded scenes. In *AAAI*, 2008.

[32] J. Strauss, L. F. Miranda-Moreno, and P. Morency. Mapping cyclist activity and injury risk in a network combining smartphone gps data and bicycle counts. *Accident; analysis and prevention*, 83:132–42, 2015.

[33] L. Sun, Z. Yan, S. M. Mellado, M. Hanheide, and T. Duckett. 3dof pedestrian trajectory prediction learned from long-term autonomous mobile robot deployment data. *2018 IEEE International Conference on Robotics and Automation (ICRA)*, pages 1–7, 2018.

[34] M. Tan, B. Chen, R. Pang, V. Vasudevan, and Q. V. Le. Mnasnet: Platform-aware neural architecture search for mobile. *CoRR*, abs/1807.11626, 2018.

[35] E. J. Topol. *The patient will see you now: the future of medicine is in your hands*. Tantor Media, 2015.

[36] C. Urmson et al. Self-driving cars and the urban challenge. *IEEE Intelligent Systems*, 23(2), 2008.

[37] A. Vemula, K. Muelling, and J. Oh. Social attention: Modeling attention in human crowds. *2018 IEEE International Conference on Robotics and Automation (ICRA)*, pages 1–7, 2018.

[38] O. Vinyals, A. Toshev, S. Bengio, and D. Erhan. Show and tell: Lessons learned from the 2015 mscoco image captioning challenge. *IEEE Transactions on Pattern Analysis and Machine Intelligence*, 39(4):652–663, 2017.

[39] E. A. Wan and R. Van Der Merwe. The unscented kalman filter for nonlinear estimation. In *Adaptive Systems for Signal Processing, Communications, and Control Symposium 2000. AS-SPCC. The IEEE 2000*, pages 153–158. Ieee, 2000.

[40] K. Yamaguchi, A. C. Berg, L. E. Ortiz, and T. L. Berg. Who are you with and where are you going? In *CVPR 2011*, pages 1345–1352, June 2011.

[41] X. Zhang, X. Zhou, M. Lin, and J. Sun. Shufflenet: An extremely efficient convolutional neural network for mobile devices. In *The IEEE Conference on Computer Vision and Pattern Recognition (CVPR)*, June 2018.

[42] B. D. Ziebart, A. Maas, J. A. Bagnell, and A. K. Dey. Maximum entropy inverse reinforcement learning. In *Proceedings of the 23rd National Conference on Artificial Intelligence - Volume 3*, AAAI'08, pages 1433–1438. AAAI Press, 2008.

[43] B. Zoph and Q. V. Le. Neural architecture search with reinforcement learning. *CoRR*, abs/1611.01578, 2016.